

1 **Biogeochemical processes in a clay formation in situ experiment: Part F –**
2 **Reactive transport modelling**

3
4 **Christophe Tournassat^{1*}, Peter Alt-Epping², Eric C. Gaucher¹, Thomas Gimmi^{2,3}, Olivier**
5 **X. Leupin⁴ and Paul Wersin⁵**

6 ¹ BRGM, French Geological Survey, Orléans, France

7 ² Rock-Water Interaction Group, Institute of Geological Sciences, University of Bern,
8 Switzerland

9 ³ Laboratory for Waste Management, Paul Scherrer Institut, Villigen, Switzerland

10 ⁴ NAGRA, CH-5430 Wettingen, Switzerland

11 ⁵ Gruner Ltd., CH-4020 Basel, Switzerland

12 *Corresponding author and mailing address:

13 Christophe Tournassat

14 BRGM

15 Environment and Process Division (EPI/MIS)

16 3 Avenue Claude Guillemin

17 45060 Orléans Cedex 2, France

18 E-mail: c.tournassat@brgm.fr

19 Tel: +33 (0)2 38 64 47 44

20 Fax: +33 (0)2 38 64 30 62

hal-00597122, version 1 - 31 May 2011

21

22 **Abstract**

23

24

25

26

27

28

29

30

31

32

33

34

35

36

37

38

39

40

Reactive transport modelling was used to simulate solute transport, thermodynamic reactions, ion exchange and biodegradation in the Porewater Chemistry (PC) experiment at the Mont Terri Rock Laboratory. Simulations show that the most important chemical processes controlling the fluid composition within the borehole and the surrounding formation during the experiment are ion exchange, biodegradation and dissolution/precipitation reactions involving pyrite and carbonate minerals. In contrast, thermodynamic mineral dissolution/precipitation reactions involving aluminosilicate minerals have little impact on the fluid composition on the time-scale of the experiment. With the accurate description of the initial chemical condition in the formation in combination with kinetic formulations describing the different stages of bacterial activities, we succeeded in reproducing the evolution of important system parameters, such as the pH, redox potential, total organic carbon, dissolved inorganic carbon and sulphate concentration. Leaching of glycerol from the pH-electrode may be the primary source of organic material that initiated bacterial growth, which caused the chemical perturbation in the borehole. Results from these simulations are consistent with data from the over-coring and demonstrate that the Opalinus Clay has a high buffering capacity in terms of chemical perturbations caused by bacterial activity. This buffering capacity can be attributed to the carbonate system as well as to the reactivity of clay surfaces.

41

42 **1. Introduction**

43 Over the past two decades, reactive transport models have evolved as valuable diagnostic and
44 prognostic tools and have made a significant contribution to elucidating the inherently complex
45 dynamics of natural and engineered environments (Appelo, 1994; Steefel et al., 2003; Steefel et
46 al., 2005; Gaucher and Blanc, 2006; Appelo et al., 2008; Gaus et al., 2008; Han et al., 2010).

47 These models provide the theoretical framework for simulating coupled thermal-hydraulic-
48 chemical-biological processes within earth systems. As such, these models constitute a basis for
49 testing concepts and hypotheses and for integrating new experimental, observational and
50 theoretical knowledge about geochemical, biological and transport processes (e.g. Steefel and
51 Lichtner, 1994; Lichtner et al., 1996; Appelo et al., 1998; Maher et al., 2009).

52 The Porewater Chemistry (PC) experiment in the Mont Terri Laboratory was designed to
53 improve our understanding of the compositional characteristics and the buffering mechanisms of
54 the porewater in the Opalinus Clay. For that purpose, a vertical borehole of 52 mm diameter was
55 drilled to a depth of 10.10 m. The bedding dips at an angle of about 45° to the SE. The first 5
56 meters of the borehole were drilled with air. For the remaining 5.1 m, nitrogen was used in order
57 to minimise ingress of molecular oxygen and hence oxidation of pyrite and organic matter around
58 the borehole wall. Immediately after drilling, the borehole was filled with Ar. The downhole
59 equipment including the 4.5 m long screen made of porous (40 µm mesh size) low pressure
60 polyethylene with a porosity of 0.3 and a 0.33 m long hydraulic mechanical packer was emplaced
61 into the borehole. The remaining part of the borehole was filled with epoxy resin (Sikadur 52).

62 The borehole was filled with synthetic porewater (2.8 L) which had been previously
63 saturated with an Ar/CO₂ gas mixture corresponding to a pCO₂ of 10^{-3.5} bar, as in air. This
64 synthetic porewater was traced to keep track of transport-controlled exchange of solutes between

65 the borehole and the surrounding formation. More details about the design and results of the
66 experiment are summarized in Wersin et al. (This Issue-a). The original focus of this experiment
67 was to obtain high-quality data on the porewater composition and thus to reduce uncertainties in
68 pH/pCO₂ and Eh. However, unexpected microbial activity in the borehole observed after about
69 nine months led to a revised research program with the following objectives:

- 70 i. to identify biogeochemical processes occurring in the borehole and describe these
71 quantitatively
- 72 ii. to obtain diffusion parameters of injected conservative tracers
- 73 iii. to identify the source of organic carbon for microbial degradation
- 74 iv. to draw conclusions on the findings with regard to conditions of the clay host rock around a
75 nuclear waste repository

76 To understand the complexity of processes and to identify and/or quantify crucial system
77 parameters of the PC experiment, modelling efforts were initiated by different groups involved in
78 the project. These efforts were only loosely coordinated and different groups were allowed to use
79 a software package of their choice and were free to decide on how to approach the task.
80 Consequently, it was never expected that the different groups would produce exactly the same
81 results. A summary of these modelling efforts can therefore only touch on some of the aspects
82 that had to be taken into account by the groups during the design of their model (e.g. model
83 dimensions and geometry, initial and boundary conditions, choice of parameters, choice of
84 relevance) and the reasons for differences in the model outputs.

85 The following section 2 aims at giving an overview of the reactive transport simulations
86 performed over the course of the PC-experiment. This overview serves as an introduction to a
87 model, discussed in detail in section 3 of the paper, that is almost fully capable of reproducing the
88 evolution of the borehole fluid during the five years of the experiment, as well as the observations

89 made on the over-core samples. The geochemical and transport properties of the Opalinus clay
90 formation are then discussed in the light of modelling results.

91

92

93 **2. Overview of previous reactive transport simulations of the PC experiment**

94 Over the course of the PC experiment, reactive transport models that couple diffusive transport
95 with chemical reactions were designed and simulations were carried out in a collective effort by
96 different groups involved in the PC experiment. The aim was to develop models that reproduce
97 not only the time series of tracer concentrations but also time series of reactive species and the
98 evolution of the redox state and the pH of the borehole fluid. A model that successfully
99 represents the measured time series of borehole fluid compositions can then be used to identify
100 critical processes and to quantify system parameters and properties within the borehole as well as
101 in the surrounding rock. Furthermore, a working model can be used to make predictions about the
102 system's behaviour in the future and/or to test what-if scenarios that assess the system's response
103 to different physical or chemical conditions (ANDRA, 2005).

104 Common to all reactive transport models was the incorporation of the processes that were
105 thought to control the chemical evolution of the system: diffusive transport, ion exchange,
106 biodegradation and mineral precipitation/dissolution reactions. Even though these were
107 considered the processes driving the chemical evolution of the system, relatively little was known
108 about the relative importance of each of these processes and if and how these processes interact.
109 One aim of coupled modelling was to elucidate some of these issues.

110 Integrating transport and chemistry into a model entails a much larger number of system
111 parameters that need to be constrained than in a model that considers non-reactive transport
112 alone. Because few constraints were available for conditions in the surrounding rock, values for

113 critical parameters regarding conditions outside the borehole could only be based on “educated
 114 guesses” and were therefore associated with a large degree of uncertainty (see discussion in
 115 Gaucher and Blanc, 2006). Owing to this uncertainty and other factors, which include among
 116 many others: 1) the use of different software packages and geochemical datasets, 2) the choice of
 117 parameters and the degree of detail, 3) the choice and the mathematical implementation of
 118 processes and the couplings between them, 4) the choice of initial and boundary conditions, 5)
 119 species dependent or independent diffusion, 6) uniform or species dependent accessible
 120 porosities, it was expected that the results from different modelling efforts could show substantial
 121 differences but should agree at least qualitatively and in some aspects quantitatively.

122 The earliest simulations that couple diffusive transport with chemical reactions were
 123 carried out by Arcos et al. (2003). Reactive transport was modelled in one dimension with the
 124 PHREEQC (Parkhurst and Appelo, 1999) code. These simulations already included the most
 125 important processes that were thought to control the chemistry of the porewater: the degradation
 126 of organic matter via sulphate reduction, ion exchange reactions and mineral
 127 precipitation/dissolution reactions. Of these processes, the degradation of organic matter was
 128 thought to be that which dominates the behaviour of the system in agreement with preliminary
 129 microbiological analyses (Stroes-Gascoyne et al., This Issue). Biodegradation was formulated as



131
 132 and incorporated into the model via a Monod-type rate equation.

133 Overall, the model was able to reproduce on-line measurements of critical parameters
 134 such as the pH and Eh reasonably well and confirmed the significance of biodegradation as the
 135 most prominent process in controlling the redox evolution of the system. Discrepancies between

136 measured and modelled data, in particular those related to sulphate and inorganic carbon, were
 137 attributed to the over-simplification of the formulation for organic matter degradation, the
 138 selection of the type of dissolved organic matter and the choice of kinetic parameters used in the
 139 degradation reactions.

140 Tournassat and Gaucher (2004) used the PHAST code (Parkhurst et al., 2004) to simulate,
 141 in 1D, the evolution of the borehole fluid composition by using constraints from isotopic data
 142 (e.g. $\delta^{13}\text{C}$), dissolved methane, the SO_4^{-2} concentration, the pH and the alkalinity. They
 143 concluded that methanogenic and sulphate reducing bacteria in the borehole led to a redox
 144 zonation that causes methanogenesis and methane oxidation to occur simultaneously. The redox
 145 state of the system is controlled by the S(-2)/S(+6) couple, whereby the S(-2) and S(+6) activities
 146 are buffered by pyrite (FeS_2) and a Fe-carbonate-phase (FeCO_3). The authors suggested that the
 147 system is in a redox disequilibrium that is used by sulphate-reducing bacteria to produce
 148 methane, acetate and various organic acids.

149 Grandia et al. (2006) used PHREEQC to implement a kinetic formulation for the
 150 degradation of acetone through a carboxylation process:



152 and a Monod-type rate equation for the subsequent degradation of acetate to carbonate ions via
 153 sulphate reduction:



156

157 The production of HS^- leads to the precipitation of an amorphous FeS-phase, which
158 controls the Fe concentration in the borehole. All rate parameters in the biodegradation process
159 were adjusted to match the measured data from the PC experiment and the simulations were able
160 to reproduce many aspects of the evolving system.

161 Alt-Epping et al. (2006) used FLOTRAN (Lichtner, 2007) to run simulations of a
162 cylindrical model with radial coordinates, which accounted for the oblique angle between the
163 borehole and the bedding. These simulations were fully coupled, which implies that these
164 simulations also considered the feedback between porosity changes following mineral
165 dissolution/precipitation reactions and diffusive transport. This study incorporated many
166 parameters and built on results from previous studies: the formulation and selectivity coefficients
167 for ion exchange were taken from Tournassat and Gaucher (2004) and biodegradation was
168 formulated in an analogous manner to that of Grandia et al (2006). Simulations included a
169 sensitivity analysis that compared different model outcomes as a function of the initial borehole
170 fluid composition.

171 To elucidate the importance of individual reaction processes (ion exchange,
172 biodegradation, mineral dissolution/precipitation), different model scenarios included a
173 successive increase in model complexity, from the implementation of a single process only to the
174 implementation of all reaction processes and a full coupling between them. The results from the
175 simulations showed that the different initial compositions of the borehole fluid (scenarios 1-3)
176 have relatively little impact on the evolution of the system. Without ion exchange or
177 biodegradation, the reactivity of the system is low, which is consistent with very small volumes
178 of calcite, dolomite and siderite precipitation (Figure 1). Species concentrations in the borehole
179 either increase or decrease monotonously, which indicates that these changes are primarily
180 controlled by diffusive exchange with the surrounding rock (Figure 2).

181 In contrast, after implementing biodegradation and ion exchange, the evolution of the
182 fluid composition in and around the borehole becomes more complex and the system has not
183 attained steady state after 1426 days. The system is more reactive, which is reflected in a larger
184 amount of precipitated carbonate minerals. The implementation of biodegradation reproduces one
185 of the key characteristics of the borehole fluid, which is the decrease in sulphur over time (Figure
186 2). In the borehole, organic matter reduces sulphate to sulphide, which subsequently diffuses
187 outward into the formation where it precipitates as pyrite (Figure 1). The uptake of sulphide into
188 pyrite outside the borehole steepens the total sulphur concentration profiles, thus enhancing
189 outward diffusion and causing a decrease in the total sulphur concentration in the borehole fluid
190 (Figure 2).

191 These results demonstrate the buffering capacity of the system, which is due primarily to
192 ion exchange and the buffering by carbonate phases. Biodegradation exerts the strongest impact
193 on the evolving fluid composition and causes the precipitation of pyrite. These simulations were
194 successful in describing qualitatively the processes occurring in the borehole and the surrounding
195 formation. The simulations also suggest that by selecting only those constituents and processes
196 that are relevant to the chemical evolution of the system, it is possible to design a “minimal”
197 model that is simple yet fully capable of reproducing quantitatively the evolution of the borehole
198 fluid during the five years of this experiment. This model is presented in the following sections.

199

200 **3. A simplified reactive transport model**

201 *3.1 Overview of the proposed reactive transport model*

202 As stated above, the aim of this modelling exercise was to develop a “minimal” model capable of
203 reproducing the chemical evolution of the PC experiment, i.e. the chemical evolution of
204 compounds that are coupled with each other through the simultaneous occurrence of biological

205 transformation of solute or solid compounds, in-diffusion and out-diffusion of solute species and
206 precipitation/dissolution of minerals (in the borehole and in the formation).

207 This section aims at giving an overview of the concepts and parameters used in the model. Each
208 of these parameters, including their calibration, are then discussed in the following section 4.

209 Mainly because biological activities are highly non linear, processes occurring in the
210 experimental borehole could not be modelled using a purely mechanistic approach without fitting
211 parameters. Thus, it is not within the scope of this paper to try to present a biological mechanistic
212 model.

213 Different events during the course of the experiment (e.g. water sampling, leakage and
214 others) caused changing boundary conditions. As discussed elsewhere in this series of papers, the
215 major changes in the water chemistry during the PC experiment included decreasing
216 concentrations of bromide, deuterium and sulphate and increases in the organic carbon and total
217 dissolved carbonate contents. The changes in the bromide and deuterium contents were expected
218 because the test water was spiked with both of them to act as tracers. The measured
219 concentrations of these tracers in the borehole are shown in Part A, Figure 7. They differ
220 considerably from those expected in that the concentrations in samples taken late in the
221 experiment, instead of continuing to decreasing asymptotically to the low concentrations in the
222 formation water, began to increase toward those of the initial test water. This behaviour could be
223 linked to the experimental needs, where the chemical composition of the water in the borehole
224 was changed through dilution of the borehole water with volumes of synthetic water (high
225 concentration of bromide, but also zero concentration of sulphides, etc.) introduced into the
226 system to compensate the losses due to sampling or leakages. As a second consequence, these
227 events led also to changes in the concentration gradients between the borehole and the
228 surrounding formation, hence having an effect on the solute diffusion in/from the formation. It

229 was then necessary to take these events into account in the reactive transport calculation to
230 achieve good mass balance. This was achieved by building a model with several restarts after
231 having changed the conditions in the borehole through mixing of the borehole water with
232 synthetic porewater.

233 Changing boundary conditions as a function of time had to be considered also for
234 bacterial activity. Biological analyses (Stroes-Gascoyne et al., This Issue) showed that different
235 bacterial strains with different sources of energy (e.g. sulphate reduction vs. methanogenesis)
236 were active in the borehole. Four different periods of bacterial activity can be discerned in Figure
237 3. Phase 1 is characterized by almost no release of organic matter into the system. As a
238 consequence, a low bacterial activity is expected. A significant release of organic matter different
239 from acetate is observed in phase 2, while in phase 3 there is a release of organic matter and a
240 concomitant transformation into acetate. In phase 4, the organic matter concentration in the
241 borehole decreases due to degradation into inorganic carbon and diffusion into the surrounding
242 formation, providing that the organic matter release in the borehole stopped or decreased
243 drastically. Figure 4 also shows that phase 4 must itself be subdivided into two periods for the
244 description of a bloom of methanogenesis before it slows down. This event has been recorded in
245 biological analysis through the presence of active methanogenic bacteria at the end of the
246 experiment.

247 Figure 3 clearly shows that acetate was not the primary source of organic carbon in the
248 system because acetate concentration is well below total or dissolved organic carbon
249 concentration before phase 3. Acetate must therefore be considered as a secondary product of the
250 bacterial activity. This secondary product can itself be degraded into inorganic carbon, as will be
251 shown later. The nature of the primary source organic matter that was released into the borehole
252 and then transformed into acetate was the subject of much controversy over the course of the

253 experiment: among the possible candidates, acetone ($\text{CH}_3\text{-CO-CH}_3$), which was used for cleaning
254 the filters before the experiment, was long preferred until modern carbon measurements on
255 dissolved organic carbon revealed that the carbon source was a modern one (De Cannière et al.,
256 This issue). After thoroughly scrutinizing the potential sources of modern carbon in the system,
257 De Cannière et al. came to the conclusion that glycerol ($\text{C}_3\text{H}_8\text{O}_3$), originating from the gel pH-
258 electrode, was the most probable candidate as the primary source of organic carbon in the system.

259 The two samples during phase 3 exhibited acetate concentration of the same level as total
260 organic matter. Moreover, these concentrations increased during phase 3. This observation can
261 only be explained by considering that the primary source of organic carbon, once released into
262 the borehole water, is immediately converted into acetate. From a modelling conceptual point of
263 view, this behaviour is equivalent to the presence of a “solid” source of carbon that is not
264 released into solution but is directly degraded into acetate. If we consider that glycerol from the
265 electrode is indeed the primary source of carbon, this could be explained by the presence of an
266 intense bacterial activity in the vicinity of the electrode degrading glycerol into acetate. On the
267 contrary, during phase 2, total organic carbon concentration is much higher than acetate
268 concentration, evidencing a release from the electrode that is faster than the consumption by
269 surrounding bacteria, possibly because the initial population of active bacteria was very small. As
270 a consequence, organic matter releases in the system were modelled by three distinct kinetic rates
271 accounting for these three situations: (i) a rate for glycerol (or another organic compound) release
272 into solution, (ii) a rate for its degradation into acetate and (iii) a rate for direct release of acetate
273 into solution accounting for the rapid conversion of glycerol (or another organic compound) into
274 acetate at the source term.

275 These rates were arbitrarily changed as a function of time in order to accurately reproduce
276 the data shown in Figure 3. This approach must be seen as a purely fitting approach that is

277 justified because the interest of the modelling was to understand the response of the system to the
 278 bacterial activity.

279

280 3.2. Numerical modelling methods

281 3.2.1 Geometry and transport

282 In the modelling approach that follows, the experimental borehole was considered to be a perfect
 283 cylinder. Diffusion taking place at the bottom and the top ends of the cylinder was neglected in
 284 comparison to radial diffusion owing to the low value of their surface area as compared to radial
 285 surfaces. Anisotropy of diffusion due to the bedding of the rock (Arcos et al., 2004; Van Loon et
 286 al., 2004a; Van Loon et al., 2004b) was not taken explicitly into account. With this
 287 approximation, the system turned into a 1D radial model. This type of geometry can be
 288 implemented in PHREEQC using the “-stagnant_cells” option. (Parkhurst and Appelo, 1999;
 289 Appelo, 2007; Appelo and Wersin, 2007). Transport by diffusion is solved at each time step by
 290 mixing iteratively adjacent cells (n and $n+1$) following the relationship:

291

$$\text{mix}f_{n,n+1} = \varepsilon \times D_p \times \Delta t \times \frac{A_{n,n+1}}{h_{n,n+1} \times V_n} \times f_{bc} \quad \text{Equation 1}$$

292 where $\varepsilon \times D_p$ is the harmonic mean of the effective diffusion coefficient, i.e.:

293

$$\varepsilon \times D_p = 2 \frac{\varepsilon_n \times D_{p,n} \times \varepsilon_{n+1} \times D_{p,n+1}}{\varepsilon_n \times D_{p,n} + \varepsilon_{n+1} \times D_{p,n+1}} \quad \text{Equation 2}$$

294 where Δt is the time step (s), $A_{n,n+1}$ is the shared surface area among cells n and $n+1$ (m^2), $h_{n,n+1}$
 295 is the distance between midpoints of the cells n and $n+1$ (m), V_n is the water volume in cell n for

296 which the concentration change is calculated (m^3), and f_{bc} is a correction factor that equals 2 for
297 constant concentration (end cell of the system) and 1 otherwise (inner cell of the system with
298 closed boundary). ε_n (-) is the porosity of cell n. $D_{p,n}$ is the pore diffusion coefficient of cell n (m^2
299 s^{-1}). If no surface diffusion (in the electrostatic double layer at charged mineral surfaces) is
300 considered, the pore diffusion coefficient is related to the effective diffusion coefficient (D_e) by
301 the relationship:

$$D_{e,n} = \varepsilon_n \times D_{p,n} \quad \text{Equation 3}$$

303 The borehole was modelled using only one numerical cell representative of the ring
304 volume containing the test water (the inner part of the borehole was filled with instrumental
305 devices). Surface to volume ratios between adjacent cells were calculated according to the
306 diameter of the borehole (0.052 m) and the size of each numerical cell. The Opalinus Clay
307 formation was represented by 33 cells extending 1.5 m into the clay formation. Grid size was
308 refined when approaching the borehole/formation interface: cell sizes ranged from 0.002 m at the
309 interface up to 0.2 m in the clay formation. Considering the total length of the borehole (4.63 m),
310 this corresponds to a porous rock volume of $0.0016 m^3$ for the cell at the interface and $8.3 m^3$ for
311 the last cell in the clay formation. Transport parameters were fitted according to the Br and
312 deuterium diffusion profiles using the multicomponent diffusion option of PHREEQC (different
313 D_p values can be attributed to different solutes in the system). All dilution events (sampling and
314 leakages reported in Wersin et al., This issue-a) were taken into account.

315

316 3.2.2 Chemistry Database

317 The BRGM Thermoddem database (<http://thermoddem.brgm.fr/index.asp?langue=GB>) was used
318 for chemical species and minerals solubility given the need for reliable thermodynamic data of
319 clay minerals. Preliminary simulation runs made it possible to simplify calculations by removing
320 unnecessary solute species. The database used for the simulation is given in Electronic Annex 1.

321

322 3.3. *Boundary conditions*

323 3.3.1 Anion concentration and accessible porosity

324 Because of the out-diffusion of chloride at the Lias and Dogger boundaries, porewaters of
325 the Opalinus Clay at Mont Terri show a distinct diffusion profile through the formation (See
326 Figure 2 in Wersin et al., This issue-a). The stability of the Cl + Br concentration profile due to
327 diffusion of Br from the borehole in the formation and Cl from the formation in the borehole
328 confirmed that porewater chloride concentration was about 0.3 mol/L (Figure 5). Sulphate
329 concentration was adjusted to match the Cl/sulphate seawater ratio in agreement with porewater
330 modelling results (Pearson et al., This issue).

331 Total water loss at 105°C ($7.42 - 8.4 \text{ kg}_{\text{water}} \text{ kg}_{\text{rock}}^{-1}$) together with rock bulk density
332 determination ($2.38\text{-}2.4 \text{ kg dm}^{-3}$) enabled Koroleva et al. (This issue) to determine a mean total
333 porosity of 0.19. This value is also in agreement with reported grain density of 2.7 kg dm^{-3}
334 (Pearson et al., 2003, Table A9.12). This porosity value is high when compared to previously
335 reported values measured with the same method (Pearson et al., 2003, Table A9.12). However, it
336 is still in agreement with porosity values obtained from HTO diffusion experiments: for instance
337 Van Loon et al. (2003) reported values up to 0.2. According to (i) this porosity value, (ii) the total
338 chloride content that can be leached from the sample and (iii) the Cl concentration in the
339 porewater (as given by the final concentration of the test water), Koroleva et al. (This issue) also
340 calculated that anion accessible porosity represents ~75% of total porosity. This value is higher

341 than the usually reported mean value of ~50-60%, but still in reasonable agreement with the
 342 range of variation reported in the literature (40-70%, Van Loon et al., 2003; Van Loon et al.,
 343 2004a; Van Loon et al., 2007). As a consequence, it was decided to consider this measured value
 344 in the modelling exercise. In the following, an anion accessible porosity of 0.14 corresponding to
 345 0.06 kg_w/kg_r will be used and the remaining 0.02 kg_w/kg_r must be considered as “surface water”
 346 (Appelo and Wersin, 2007; Appelo et al., 2008).

347

348 3.3.2. Major cations (Na, K, Ca, Mg, Sr) and cation exchange

349 A cation exchange reaction can be represented by the following reaction equation, in the case of a
 350 Na⁺/Me^{z+} binary system (Me = K, Ca, Mg or Sr):

351



352

353 where X⁻ represents a negatively charged surface site. The selectivity coefficient of this reaction
 354 is $K_{GT}^{Na/Me}$:

$$K_{GT}^{Na/Ca} = \frac{\{Na^+\}^z}{\{Me^{z+}\}} \times \frac{E_{Me}}{E_{Na}^z} \quad \text{Equation 4}$$

355

356 Where E values are charge fractions on the exchanger.

357 The over-coring analysis showed that cation exchanger composition is very constant as a function
 358 of borehole distance (Koroleva et al., This issue). In these conditions, Equation 4 implies that the

359 ratio of solute activity $\frac{\{Na^+\}^z}{\{Me^{z+}\}}$ is also constant. This can be verified in Figure 6.

360 The exchange selectivity coefficient of Na/Me exchange reactions can then be calculated
361 from exchanger population analysis and borehole sample data (Table 1). These values can be
362 compared to those predicted by the illite and smectite exchanger models given by Tournassat et
363 al. (Tournassat et al., 2007; Tournassat et al., 2009). The present exchange selectivity coefficients
364 can be explained by a combination of illite and smectite surfaces: modelled Na/K selectivity
365 coefficients are lower than the measured selectivity coefficient for illite/smectite mixed layer
366 minerals (I/S). This observation is in agreement with the recommendation of Tournassat et al.
367 (2009) to increase the Na/K coefficient by 0.2 – 0.4 \log_{10} unit for I/S surfaces. Exchange
368 selectivity coefficients are also in agreement with those calculated at another location with the
369 same chlorinity (BWS-A1), while they are slightly different for a location with lower chlorinity
370 (BWS-A3) (Pearson et al., This issue).

371 In the following, the $\log_{10}K_{GT}$ value calculated from borehole and core samples (first
372 column of Table 1) will be used to run the simulations.

373
374 3.3.3. Porewater chemistry

375 Initial porewater chemistry was calculated at 25°C with the model presented in Pearson et al.
376 (This issue) and with the parameters given above. The minerals considered at equilibrium with
377 the formation porewater were: quartz, calcite, siderite, chlorite (Chlorite-CCa-2), illite
378 (Illite_IMt2) and pyrite. Chosen chlorite and illite data were originally obtained from calorimetric
379 measurements (Gailhanou et al., 2007; Gailhanou et al., 2009). Porewater modelling results are
380 given in Table 2 **Erreur ! Source du renvoi introuvable.**

381

382 3.3.4 HDO and Br⁻ diffusion

383 Diffusion parallel to the bedding of Opalinus Clay from Mont Terri has already been
384 studied at the laboratory scale (Van Loon et al., 2004a) as well as in in-situ experiments (Van
385 Loon et al., 2004b). Van Loon et al., 2004b report a diffusion coefficient (D_p) of $1.1 \cdot 10^{-10}$ and 2.7
386 $10^{-10} \text{ m}^2 \text{ s}^{-1}$ for I^- and HTO respectively. Together with the measured accessible porosity
387 (Koroleva et al., This issue), these values were used in our calculations and then slightly adjusted
388 to better match the data. A good fit was obtained with D_p of $0.9 \cdot 10^{-10}$ and $2.4 \cdot 10^{-10} \text{ m}^2 \text{ s}^{-1}$ for Br^-
389 and HDO respectively (Figure 7).

390 Koroleva et al. (This issue) report spatial profiles of Br and Cl concentrations in the
391 immediate vicinity (first 17 centimetres) of the borehole. Even though the data, in particular the
392 data for Cl^- , are associated with a relatively large degree of uncertainty, there appears to be a
393 discrepancy between the computed (with diffusivities estimated from time-series of tracer
394 concentrations in the borehole fluid) and measured spatial profiles (Figure 7, lower right panel).
395 It is not easy to decide whether this shift is significant or not. If significant, this shift would
396 suggest the presence of a disturbed zone surrounding the borehole having enhanced diffusion
397 properties (Cartalade et al., 2007). Considering the overall good agreement of the model and the
398 measured data and their associated uncertainty, the possibility of a disturbed zone is not further
399 discussed.

400 In the following models, a porosity corresponding to the volume of 75% of the total water
401 content (i.e. volumetric porosity = 0.14) was assumed for the entire rock formation. In the
402 proposed reactive transport model, this porosity applies not only to anions but also to positively
403 charged and neutral species for simplicity and calculation time saving reasons. By the way,
404 considering the total porosity instead of the reduced porosity for HDO transport has little effect
405 on the calculated HDO concentrations as a function of time in the borehole (Figure 7). It is
406 possible to consider different D_p for different solute species using the multi-component diffusion

407 option of PHREEQC (Appelo and Wersin, 2007). Differences in D_p originate from differences in
 408 the diffusion coefficient in pure water (D_0) and tortuosity (τ) for different solute species. For each
 409 species i , the relationship $D_p = \tau D_0$ applies. In the present studies, D_0 values from the Phreeqd.dat
 410 database were considered together with a tortuosity factor calculated from experimental D_p for Br
 411 and HTO: we set the tortuosity (τ) for anions and neutral species as $\tau_{anions} = D_p(Br)/D_0(Br)$ and
 412 $\tau_{neutral} = D_p(HDO)/D_0(HDO)$. D_0 for OH^- and H^+ were set to the value of HDO for calculation time
 413 saving reasons. As a further simplification of the system, we considered that the same tortuosities
 414 τ_{anions} applied to all of the anions, independently of their charge and $\tau_{neutral}$ to both neutral species
 415 and cations. Cations are expected to have lower tortuosities than neutral species (Appelo and
 416 Wersin, 2007) but this effect was neglected.

417

418 3.4. Borehole conditions

419 3.4.1 Biological activity kinetic parameters

420 Once the solute species diffusion properties were fixed, six kinetic parameters for material
 421 degradation and bacterial activity could be fitted: three of them account for the release of the
 422 primary organic matter and its transformation into acetate (see section 2); two others are for
 423 sulphate reduction/acetate oxidation and the last one is for methanogenesis. Each of these
 424 parameters was constrained by measured data:

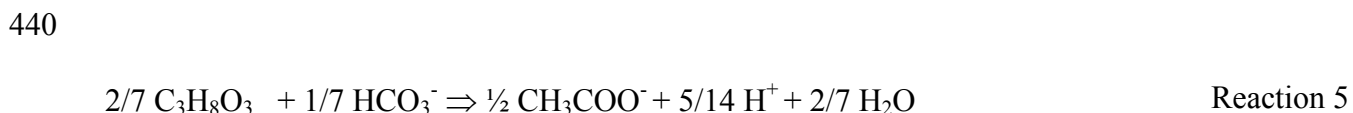
- 425 • The release rate of primary organic carbon source in solution can be computed through
 426 the difference between TOC (total organic carbon) and acetate concentrations.
- 427 • The degradation rate of this organic carbon together with the degradation rate of a “solid”
 428 carbon source into acetate was fitted with the acetate concentrations as a function of time.

- 429 • The sulphate reduction rate (through acetate oxidation) was constrained by sulphate
430 concentration as a function of time.
- 431 • The rate of methane production from acetate degradation was given by the methane
432 concentration profile as a function of time.

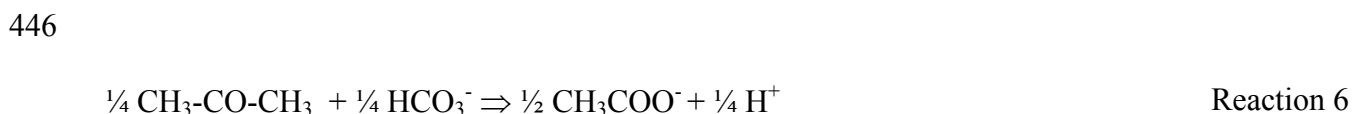
433

434 As stated in the introduction, it was not within the scope of this work to describe the
435 system with all of the intermediate degradation products and no attempt has been made to find
436 them in the literature. Measurable initial and final products solely were considered, as well as
437 zero-order kinetic reactions. Bacteria are considered here only as catalysts for thermodynamically
438 possible reactions.

439 Glycerol (described as $C_3H_8O_3$) transformation into acetate was described with:



441 Even though it is now clear that the source of carbon in the system was glycerol that leached
442 from the electrode (De Cannière et al., This issue), the question regarding the nature of this
443 source was also addressed through this reactive transport model exercise by considering two
444 other potential sources of carbon. One of these potential sources was acetone that could have
445 entered into the system after the filter cleaning procedure (De Cannière et al., This issue):



447 The other potential source was natural organic matter present in the formation, taken here
 448 as a generic CH₂O formula:



450 The sensitivity of the modelling result to the considered source of carbon could then be tested.
 451 Acetate degradation during sulphate reduction was described with



453 and methanogenesis with:



455

456 Table 1 in Electronic Annex 2 gives the fitted parameters for all of these reactions. Reaction 5 to
 457 Reaction 9 were normalized to ½ acetate (corresponding to 1 organic carbon atom). Changes in
 458 kinetic rates were defined at each experimental event.

459 Figure 8 shows the good agreement (because fitted) between modelled concentrations in
 460 the borehole as a function of time for organic compounds, sulphate and methane.

461

462 3.4.2 Mineral precipitation/dissolution

463 Due to the intense bacterial activity, a large amount of sulphide has been produced that has
 464 precipitated as FeS compounds and pyrite (Koroleva et al., This issue). According to speciation
 465 calculations using experimental data (pH, Fe(II) and sulphide concentration when available),
 466 pyrite was oversaturated. As a consequence, pyrite could not be considered at equilibrium in the
 467 simulation. According to the fast kinetic of precipitation for FeS in the experimental conditions
 468 (Rickard, 1995) with regards to the simulation time-step, we decided to consider equilibrium for
 469 a FeS compound:

470



471 The solubility K_{FeS} of the compound was fixed at the mackinawite solubility tabulated in the
 472 database ($\log_{10} K_{\text{FeS}} = -3.54$). Pyrite precipitation was considered as a kinetic process linked to
 473 the abundance of FeS (Rickard and Luther III, 2007). The rate of pyrite precipitation had little
 474 influence on the outcome of the simulation with regards to simulated Fe and sulphide
 475 concentrations in the borehole. The only effect is on the FeS/pyrite ratio of precipitated minerals.
 476 Unfortunately no quantitative data is available for this parameter.

477 Calcite was found to precipitate in the borehole as well (Koroleva et al., This issue), in
 478 agreement with its saturation index calculated from alkalinity, pH and Ca concentration (Figure
 479 9). Calcite was oversaturated during the whole of the experiment due to (i) kinetic limitation for
 480 its precipitation and/or (ii) measurement uncertainties and/or (iii) uncertainties in the database
 481 with regards to the solute complex of Ca. We took these effects into account by considering that
 482 calcite precipitated in the borehole at thermodynamic equilibrium but with a saturation index of
 483 0.2 instead of 0.

484

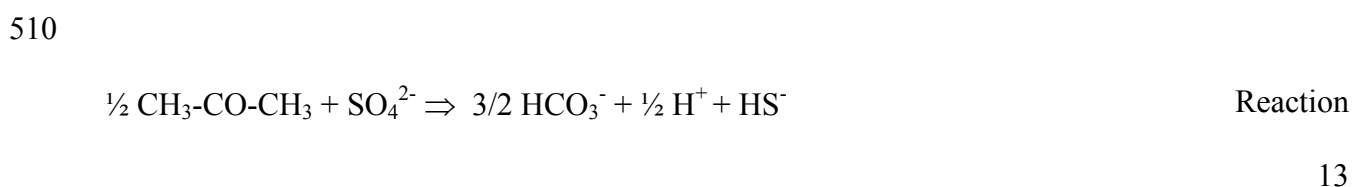
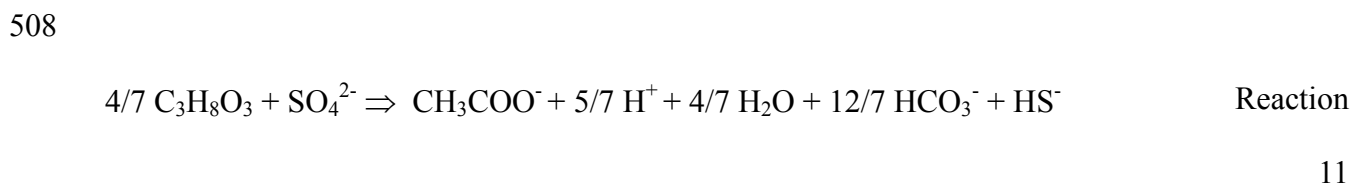
485 3.4.3 pH buffer effect of clay mineral surfaces

486 The pH buffer effect of clay minerals was taken into account by considering the clay 2-pK non
487 electrostatic model of Bradbury and Baeyens (Bradbury and Baeyens, 1997). The amounts of
488 sites were recalculated from the measured amount of illite + illite/smectite in the rock (~38%,
489 Koroleva et al., This issue). We considered that illite and smectite sites have nearly the same
490 buffer properties (Bradbury and Baeyens, 2009a; Bradbury and Baeyens, 2009b). In addition, we
491 considered that H^+ could undergo cation exchange reaction with the same affinity for the surface
492 as Na^+ (Laudelout et al., 1968; Ferrage et al., 2005). The effect of compaction on site
493 accessibility in the intact rock material was not taken into account.

494

495 **4. Results and discussion**496 4.1 *Influence of the nature of the organic matter on modelling results*

497 Once organic matter production and degradation rates have been determined, the effect of these
498 reactions can be assessed on key parameters such as pH and alkalinity. However, these
499 parameters are potentially highly buffered by the surrounding formation. In a first attempt, we
500 considered the pH buffer of the clay surfaces as described above together with the equilibrium of
501 the formation with its calcite and siderite constituents. No other mineral in the formation was
502 introduced into the model. Figure 10 shows that the consideration of CH_2O , glycerol or acetone
503 as the primary source of carbon has a significant effect on the result. Modelled alkalinity
504 increases in the order acetone < glycerol < CH_2O . Conversely, pH decreases in the order acetone
505 > glycerol > CH_2O . These relationships can be easily appreciated through the consideration of
506 combinations of reactions 11 to 14 that all concern organic matter degradation via sulphate
507 reduction:



511 For each sulphate mole that is transformed into sulphide in these reactions, glycerol produces 1.7
512 moles of bicarbonate, CH_2O , 2 moles and acetone, 1.5 moles. The evolution is similar for pH: the
513 acetone case, with 0.5 H^+ produced per mole of sulphate, exhibits logically the highest pH while
514 the CH_2O case led to the most acidic result with 1 H^+ per sulphate molecule. Glycerol produces
515 0.7 H^+ per sulphate and leads to an intermediate result between CH_2O and acetone.

516 Whereas, in all cases, pH predicted by the simulation is in general agreement with
517 measured pH, TIC and alkalinity are best reproduced with the glycerol model (Figure 10). This
518 result is in agreement with the results of De Cannière et al. (This issue), who demonstrate that
519 glycerol is the best candidate for organic source in the system.

520

521 4.2 *Influence of the pH buffer from the formation*

522 The test-case without clay surface pH buffering in the formation revealed that this buffer has an
523 important effect on the outcome of the simulation: without this buffering effect, total inorganic
524 carbon concentration increases too much while the pH is too low (Figure 11). The results remain

525 however in good agreement with the measurements. Increasing the buffering capacity by a factor
526 of three has little effect on the results (Figure 11): as a consequence, the present experiment
527 cannot be used to finely determine this buffering capacity although it confirms its existence. With
528 regard to our boundary conditions, the pH of the porewater is a parameter whose uncertainty
529 must be addressed: measured and modelled pH values up to 7.5 have been reported (Pearson et
530 al., This issue). An additional simulation was run with an initial pH of 7.4 in the porewater of the
531 formation. The alkalinity value was adjusted accordingly to achieve equilibrium with calcite
532 without changing the calcium concentration. This change has a marked effect on the modelling
533 result (Figure 11) with too low inorganic carbon concentration and too high pH: as a
534 consequence, at the location of the experiment, the pH of the porewater is rather at a value of 7
535 than 7.5. The outcome of this sensitivity analysis is summarized in Table 3.

536

537 *4.3 Iron and sulphide controls*

538 Iron and sulphide concentrations are not well reproduced by the model as a function of time
539 (Figure 12). It should be noted that the maximum concentration of sulphide at day 600 in the
540 system is in agreement with the solubility of mackinawite representative here of an “amorphous”
541 FeS compound (note that, at that time, the predicted iron concentration is not too much in error).
542 It was however neither possible to reproduce the decrease in sulphides after day 600, nor the
543 strong increase in iron concentration at day 1061. The iron and sulphide systems are highly
544 oscillatory and it is thus difficult to describe them with an equilibrium approach. In particular, the
545 peak of sulphide concentration is fully correlated with the peak in acetate concentration, although
546 the precipitated FeS in the borehole should have buffered its concentration as shown by the
547 model. Potential degassing (departure of H₂S) and introduction of atmospheric O₂ during the

548 leakage events were not taken into account in the simulations and could have played a role in the
549 control of the sulphide concentration.

550 With regards to iron, the presence of organic chelates in solution, originating from
551 bacterial activity, could be an explanation for its too high measured concentration as compared to
552 the model.

553

554 4.4 *Concentrations of major cations*

555 Major cations (Na, Ca, Mg, K, Sr) are adequately described by the model (Figure 13). This result
556 was fully expected since the porewater composition was calculated in agreement with their
557 concentrations that remained almost constant in the borehole during the experiment. It may be
558 noted that the modelled calcium concentration decreases with time in the borehole and with an
559 evolution parallel to the measured concentration. A slight increase in the Ca concentration in the
560 porewater (corresponding to a small decrease in the exchange selectivity coefficient for Ca)
561 together with an increase in the saturation index of calcite would make it possible to reproduce
562 almost perfectly the data (not shown).

563

564 4.5 *Comparisons with over-coring data*

565 Mineralogical and chemical data obtained from over-coring sampling did not show
566 significant changes in the composition of the clayrock material directly surrounding the
567 experiment in spite of the dramatic changes of concentration of some elements in the borehole
568 (e.g. sulphate, sulphur, pH and total inorganic carbon). Conversely, the analysis of mineralogical
569 phases having precipitated inside the borehole revealed the high reactivity of the system. This
570 type of contrasting information between clay-rock and borehole is direct proof of the high

571 buffering capacity of the rock with regard to chemical perturbations and it can be further
572 ascertained from the analysis of reactive transport modelling outcomes.

573 The precipitation of “amorphous” sulphide mineral in the borehole together with a
574 kinetically controlled precipitation of pyrite was an input condition for the modelling. The
575 important information obtained from the modelling work is that (i) sulphide minerals can
576 effectively precipitate (from the thermodynamic and kinetic points of view) and (ii) that more
577 than 99.9% of amorphous sulphide mineral precipitated at the interface. Figure 14 illustrates the
578 presence of a zone enriched in precipitates at the borehole/clay formation interface (the y-axis is
579 in log scale). Detachment of minerals from this zone due to water circulation causing erosion of
580 the borehole wall could explain the massive presence of sulphide minerals at the bottom of the
581 borehole and in the circulation tubes at the end of the experiment. This simulation result also
582 explains why it was not possible to detect precipitation of such phases inside the clayrock
583 formation.

584 While calcite precipitation has been observed in the borehole, it was not possible to detect
585 any newly precipitated calcite in the first centimetres of the formation. The simulations are also
586 in agreement with this observation, since only the borehole shows significant change in its calcite
587 content (8.85 mmol L⁻¹ were precipitated in the borehole according to simulation results). The
588 maximum relative increase in calcite content is at the interface and accounts only for 0.3% of the
589 initial amount of calcite. Accordingly, the change of pH in the formation is rapidly buffered as
590 shown in Figure 15.

591

592 **5. Conclusions**

593 Reactive transport modelling simulation of the porewater chemistry experiment at Mont Terri
594 proved to be efficient in reproducing a complex set of chemical analyses as a function of time.

595 The good agreement between the model and the measurements performed in the borehole water
596 and also in samples from over-coring enables the following conclusions to be drawn:

597 (i) The Opalinus Clay rock formation has a high buffering capacity with regard to chemical
598 perturbation due to bacterial activity: sulphur production as well as pH decrease or alkalinity
599 increase was buffered within a few centimetres around the borehole. This buffering capacity is
600 attributed to the carbonate system as well as to the clay surfaces reactivity.

601 (ii) The chemical controls of pH and major cations and anions in Opalinus Clay porewater
602 chemistry are now well constrained (Pearson et al., This issue), enabling realistic simulations of a
603 perturbed system thanks to an accurate description of the initial unperturbed system.

604 (iii) Reactive transport models proved to be useful in discriminating between hypotheses with
605 regard to different reactive pathways (e.g. different sources of organic carbon for bacteria in this
606 experiment).

607 Of course, it is not possible to prove that the proposed model is the unique solution to the
608 system with regards to the numerous parameters that are (or could be) included. The present work
609 only shows that it is possible to reproduce all main outcomes of a chemical perturbation in a clay
610 host-rock with a model that takes into account the state of the art on chemical controls in these
611 rocks. Potential applications of this model are discussed in the next synthesis paper (Wersin et al.,
612 This issue-b).

613

614 **Acknowledgements**

615 This work was undertaken in close co-operation with, and with the financial support of, the Mont
616 Terri Consortium. We appreciate fruitful discussions with Agnes Vinsot, Suzanne Mettler, Pierre
617 De Cannière, David Arcos, Urs Mader, Nick Waber and Sim Stroes-Gascoyne during the

618 Porewater Chemistry experiment. Many thanks also to the Mont Terri team, including Christophe
619 Nussbaum and Paul Bossart (Swisstopo), for their continuous support to the project.
620

621

622 **References**

623

- 624 Alt-Epping, P., Gimmi, T., and Waber, H. N., 2006. Porewater Chemistry (PC) Experiment at
625 Mt. Terri, Switzerland: Reactive transport simulations. NAGRA Technical Note, TN
626 2006-66.
- 627 ANDRA, 2005. Référentiel du comportement des radionucléides et des toxiques chimiques d'un
628 stockage dans le Callovo-Oxfordien jusqu'à l'Homme. Dossier 2005 Argile. Agence
629 Nationale pour la gestion des déchets radioactifs, Châtenay-Malabry, France.
- 630 Appelo, C. A. J., 1994. Some Calculations on Multicomponent Transport with Cation-Exchange
631 in Aquifers. *Ground Water* **32**, 968-975.
- 632 Appelo, C. A. J., 2007. Multicomponent diffusion modeling in clay systems with application to
633 the diffusion of tritium, iodide, and sodium in Opalinus clay. Supporting information.
- 634 Appelo, C. A. J., Verweij, E., and Schäfer, H., 1998. A hydrogeochemical transport model for an
635 oxidation experiment with pyrite/calcite/exchangers/organic matter containing sand. *Appl.*
636 *Geochem.* **13**, 257-268.
- 637 Appelo, C. A. J., Vinsot, A., Mettler, S., and Wechner, S., 2008. Obtaining the porewater
638 composition of a clay rock by modeling the in- and out-diffusion of anions and cations
639 from an in-situ experiment. *J. Contam. Hydrol.* **101**, 67-76.
- 640 Appelo, C. A. J. and Wersin, P., 2007. Multicomponent diffusion modeling in clay systems with
641 application to the diffusion of tritium, iodide, and sodium in Opalinus clay. *Environ. Sci.*
642 *Technol.* **41**, 5002-5007.
- 643 Arcos, D., 2003. Porewater chemistry (PC) experiment: Results of the geochemical modelling.
644 Mont Terri Project TN 2003-18.
- 645 Arcos, D., Gimmi, T., Duro, L., and Waber, H. N., 2004. Modelling of tracer behaviour and
646 dominant reactions during the pore water chemistry (PC) experiment in the Opalinus
647 Clay, Switzerland. *11th Water-Rock Interaction Congress*, Saratoga Springs.
- 648 Bradbury, M. H. and Baeyens, B., 1997. A mechanistic description of Ni and Zn sorption on Na-
649 montmorillonite. Part II: modeling. *J. Contam. Hydrol.* **27**, 223-248.
- 650 Bradbury, M. H. and Baeyens, B., 2009a. Sorption modelling on illite Part I: Titration
651 measurements and the sorption of Ni, Co, Eu and Sn. *Geochim. Cosmochim. Acta* **73**,
652 990-1003.
- 653 Bradbury, M. H. and Baeyens, B., 2009b. Sorption modelling on illite. Part II: Actinide sorption
654 and linear free energy relationships. *Geochim. Cosmochim. Acta* **73**, 1004-1013.
- 655 Cartalade, A., Montarnal, P., Filippi, M., Mugler, C., Lamoureux, M., Martinez, J. M., Clement,
656 F., Wileveau, Y., Coelho, D., and Tevissen, E., 2007. Application of inverse modeling
657 methods to thermal and diffusion experiments at Mont Terri Rock laboratory. *Physics and*
658 *Chemistry of the Earth* **32**, 491-506.
- 659 Courdouan, A., Christl, I., Meylan, S., Wersin, P., and Kretzschmar, R., 2007. Characterization
660 of dissolved organic matter in anoxic rock extracts and in situ pore water of the Opalinus
661 Clay. *Appl. Geochem.* **22**, 2926-2939.
- 662 De Cannière, P., Schwarzbauer, J., Höhener, P., Lorenz, G., Salah, S., Leupin, O. X., and P., W.,
663 This issue. Biogeochemical processes in a clay formation in-situ experiment: Part C -

- 664 Organic contamination and leaching data in porewater chemistry experiment at Mont
 665 Terri Rock laboratory *Appl. Geochem.*
- 666 Ferrage, E., Tournassat, C., Rinnert, E., and Lanson, B., 2005. Influence of pH on the interlayer
 667 cationic composition and hydration state of Ca-montmorillonite: Analytical chemistry,
 668 chemical modelling and XRD profile modelling study. *Geochim. Cosmochim. Acta* **69**,
 669 2797-2812.
- 670 Gailhanou, H., van Miltenburg, J. C., Rogez, J., Olives, J., Amouric, M., Gaucher, E. C., and
 671 Blanc, P., 2007. Thermodynamic properties of anhydrous smectite MX-80, illite IMt-2
 672 and mixed-layer illite-smectite ISCz-1 as determined by calorimetric methods. Part I:
 673 Heat capacities, heat contents and entropies. *Geochim. Cosmochim. Acta* **71**, 5463-5473.
- 674 Gailhanou, H., van Miltenburg, J. C., van Genderen, A., Rogez, J., Greneche, J. M., Gilles, C.,
 675 Gaucher, E. C., and Blanc, P., 2009. Thermodynamic properties of ripidolite CCa-2. Part
 676 I. Heat capacities, heat contents and entropies. *Geochim. Cosmochim. Acta* **73**, 4738-
 677 4749.
- 678 Gaucher, E. C. and Blanc, P., 2006. Cement/clay interactions - A review: Experiments, natural
 679 analogues, and modeling. *Waste Management* **26**, 776-788.
- 680 Gaus, I., Audigane, P., Andre, L., Lions, J., Jacquemet, N., Dutst, P., Czernichowski-Lauriol, I.,
 681 and Azaroual, M., 2008. Geochemical and solute transport modelling for CO₂ storage,
 682 what to expect from it? *International Journal of Greenhouse Gas Control* **2**, 605-625.
- 683 Grandia, F., Domènech, C., and Arcos, D., 2006. Pore water chemistry (PC) experiment: Results
 684 of the geochemical modelling. ENVIROS report, R-2225.1.
- 685 Han, W. S., McPherson, B. J., Lichtner, P. C., and Wang, F. P., 2010. Evaluation of trapping
 686 mechanisms in geologic CO₂ sequestration: case study of sacroc northern platform, a 35-
 687 Year Co₂ injection site. *Am. J. Sci.* **310**, 282-324.
- 688 Koroleva, M., Lerouge, C., Mäder, U., Claret, F., and Gaucher, E. C., This issue. Biogeochemical
 689 processes in a clay formation in-situ experiment: Part B - Results from overcoring and
 690 evidence of strong buffering by the rock formation *Appl. Geochem.*
- 691 Laudelout, H., Van Bladel, R., Bolt, G. H., and Page, A. L., 1968. Thermodynamics of
 692 heterovalent cation exchange reactions in a montmorillonite clay. *Transactions of the*
 693 *Faraday Society* **64**, 1477-1488.
- 694 Lichtner, P. C., 2007. FLOTRAN Users Manual: Two-phase non-isothermal coupled thermal-
 695 hydrologic-chemical (THC) reactive flow and transport code, Version 2 Los Alamos
 696 National Laboratory, Los Alamos, New Mexico.
- 697 Lichtner, P. C., Steefel, C. I., and Oelkers, E. H., 1996. *Reactive transport in porous media*.
 698 Mineralogical Society of America.
- 699 Maher, K., Steefel, C. I., White, A. F., and Stonestrom, D. A., 2009. The role of reaction affinity
 700 and secondary minerals in regulating chemical weathering rates at the Santa Cruz Soil
 701 Chronosequence, California. *Geochim. Cosmochim. Acta* **73**, 2804-2831.
- 702 Parkhurst, D. L. and Appelo, C. A. J., 1999. User's guide to PHREEQC (Version 2) - A computer
 703 program for speciation, batch-reaction, one-dimensional transport, and inverse
 704 geochemical calculations *Water-resources investigations*.
- 705 Parkhurst, D. L., Kipp, K. L., Engesgaard, P., and Charlton, S. R., 2004. PHAST- A program for
 706 simulating ground-water flow, solute transport, and multicomponent geochemical
 707 reactions *Techniques and Methods 6-A8*. U.S. Geological Survey.
- 708 Pearson, F. J., Arcos, D., Boisson, J.-Y., Fernandez, A. M., Gäbler, H.-E., Gaucher, E., Gautschi,
 709 A., Griffault, L., Hernan, P., and Waber, H. N., 2003. Mont Terri project - Geochemistry

- 710 of water in the Opalinus clay formation at the Mont Terri Rock Laboratory. *Geology*
 711 *Series No. 5 Swiss Federal Office fo Water and Geology*. Bern.
- 712 Pearson, F. J., Tournassat, C., and Gaucher, E. C., This issue. Equilibrium controls on chemistry
 713 of pore water from the Opalinus Clay, Mont Terri Underground Research Laboratory,
 714 Switzerland. *Appl. Geochem.*
- 715 Rickard, D., 1995. Kinetics of FeS precipitation: Part 1. Competing reaction mechanisms.
 716 *Geochim. Cosmochim. Acta* **59**, 4367-4379.
- 717 Rickard, D. and Luther III, G. W., 2007. Chemistry of iron sulfides. *Chemical Reviews* **107**, 514-
 718 562.
- 719 Steefel, C. I., Carroll, S., Zhao, P., and Roberts, S., 2003. Cesium migration in Hanford sediment:
 720 a multisite cation exchange model based on laboratory transport experiments. *J. Contam.*
 721 *Hydrol.* **67**, 219-246.
- 722 Steefel, C. I., DePaolo, D. J., and Lichtner, P. C., 2005. Reactive transport modeling: An essential
 723 tool and a new research approach for the Earth sciences. *Earth and Planetary Science*
 724 *Letters* **240**, 539-558.
- 725 Steefel, C. I. and Lichtner, P. C., 1994. Diffusion and reaction in rock matrix bordering a
 726 hyperalkaline fluid-filled fracture. *Geochim. Cosmochim. Acta* **58**, 3595-3612.
- 727 Stroes-Gascoyne, S., Sergeant, C., Schippers, S., Hamon, C. V., Nèble, S., Vesvres, M.-H.,
 728 Barsotti, V., Poulain, S., and Le Marrec, C., This Issue. Biogeochemical processes in a
 729 clay formation in-situ experiment: Part D - Microbial analyses - Synthesis of results.
 730 *Appl. Geochem.*
- 731 Tournassat, C., Gailhanou, H., Crouzet, C., Braibant, G., Gautier, A., and Gaucher, E. C., 2009.
 732 Cation exchange selectivity coefficient values on smectite and mixed-layer illite/smectite
 733 minerals *Soil Sci. Soc. Am. J.* **73**, 928-942.
- 734 Tournassat, C., Gailhanou, H., Crouzet, C., Braibant, G., Gautier, A., Lassin, A., Blanc, P., and
 735 Gaucher, E. C., 2007. Two cation exchange models for direct and inverse modelling of
 736 solution major cation composition in equilibrium with illite surfaces. *Geochim.*
 737 *Cosmochim. Acta* **71**, 1098-1114.
- 738 Tournassat, C. and Gaucher, E., 2004. Progress in modelling PC-experiment results including
 739 thermodynamics, kinetics, micro-organism activity and isotopic fractionation
 740 considerations. BRGM/RP-53395-FR, NAGRA/TN 2004-72.
- 741 Van Loon, L. R., Glaus, M. A., and Müller, W., 2007. Anion exclusion effects in compacted
 742 bentonites: Towards a better understanding of anion diffusion. *Appl. Geochem.* **22**, 2536-
 743 2552.
- 744 Van Loon, L. R., Soler, J. M., Jakob, A., and Bradbury, M. H., 2003. Effect of confining pressure
 745 on the diffusion of HTO, $^{36}\text{Cl}^-$ and $^{125}\text{I}^-$ in a layered argillaceous rock (Opalinus Clay):
 746 diffusion perpendicular to the fabric. *Appl. Geochem.* **18**, 1653-1662.
- 747 Van Loon, L. R., Soler, J. M., Muller, W., and Bradbury, M. H., 2004a. Anisotropic diffusion in
 748 layered argillaceous rocks: a case study with Opalinus Clay. *Environ. Sci. Technol.* **38**,
 749 5721-5728.
- 750 Van Loon, L. R., Wersin, P., Soler, J. M., Eikenberg, J., Gimmi, T., Hernan, P., Dewonck, S., and
 751 Savoye, S., 2004b. In-situ diffusion of HTO, $^{22}\text{Na}^+$, Cs^+ and I^- in Opalinus Clay at the
 752 Mont Terri underground rock laboratory. *Radiochim. Acta* **92**, 757-763.
- 753 Wersin, P., Leupin, O. X., Mettler, S., Gaucher, E. C., Mäder, U., De Cannière, P., Vinsot, A.,
 754 Gäbler, H. E., Kunimaro, T., Kiho, K., and Eichinger, L., This issue-a. Biogeochemical
 755 processes in a clay formation in-situ experiment: Part A - Overview, experimental design

756 and water data of an experiment in the Opalinus Clay at the Mont Terri Underground
757 Research Laboratory, Switzerland. *Appl. Geochem.*
758 Wersin, P., Stroes-Gascoyne, S., Pearson, F. J., Tournassat, C., Leupin, O. X., and Schwyn, B.,
759 This issue-b. Biogeochemical processes in a clay formation in-situ experiment: Part G -
760 Key interpretations and conclusions. Implications for repository safety. *Appl. Geochem.*
761
762

763

764 Table 1. Calculated and predicted selectivity coefficient for Na/Me exchange on Opalinus Clay.

Exchange reaction	Calculated $\log_{10}K_{GT}$ from borehole and core sample analysis	Predicted $\log_{10}K_{GT}$ for illite surfaces (from a)	Predicted $\log_{10}K_{GT}$ for smectite surfaces (from b)	Calculated $\log_{10}K_{GT}$ for BWS-A1 samples water (from c)	Calculated $\log_{10}K_{GT}$ for BWS-A3 samples water (from c)
Na→K	1.40 ± 0.05	0.96	0.96	1.32	1.26
Na→Ca	0.78 ± 0.06	0.41	0.99	0.83	0.63
Na→Mg	0.62 ± 0.05	0.71	0.75	0.61	0.48
Na→Sr	1.14 ± 0.22	-	1.17	0.97	0.51

765 a. Tournassat et al., 2007

766 b. Tournassat et al., 2009, including effects of cation-chloride ion pairs

767 c. Pearson et al., this volume

768

769

Table 2. Modelled initial porewater composition.

	Modelled initial porewater composition	Analysed test water composition (mean of initial and final)
pH	7.01	7.74
pe	-2.74	
Elements	Concentration (mmol/kg _w)	
Cl	300	262
Br ¹	0.6	29.0
S(6)	15.0	14.8
TIC	3.16	1.3
Na	257	256
K	1.96	1.45
Ca	16.7	15.8
Mg	19.9	18.0
Sr	0.43	0.33
Fe	0.14	
Si	0.18	
Al	21.4 10 ⁻⁶	
Acetic acid ²	0.2	
Methane ³	0.035	

770 ¹ From Pearson et al., 2003771 ² From Courdouan et al., 2007772 ³ Taken at the value of the first plateau of methane concentration from day 116 to day 529

773

774 Table 3. Outcome of sensitivity analysis on organic matter source and clay pH buffer effect.

775

	Organic matter	Clay pH buffer	Comment
Simulation 1	CH ₂ O	Yes	High alkalinity, low pH
Simulation 2	Acetone	Yes	Low alkalinity, high pH
Simulation 3 = reference simulation	Glycerol	Yes	
Simulation 4	Glycerol	No	High alkalinity, low pH
Simulation 5	Glycerol	Yes × 3	Almost no effect
Simulation 6	Glycerol	Yes and initial pH = 7.4	Low alkalinity, high pH

776

777

Figure captions

778 Figure 1. Profiles of mineral volume changes over a period of 1426 days, without (A) and with
779 ion exchange and biodegradation (B) from Alt-Epping et al. (2006). The vertical line represents
780 the borehole/rock interface. The precipitation of carbonate phases, calcite, dolomite and siderite
781 along with ion exchange with clay surfaces act as buffer for the fluid composition. Increasing
782 chemical complexity leads to a larger volume fraction of carbonate minerals. Sulphate reduction
783 through biodegradation causes pyrite to precipitate.

784 Figure 2. Spatial profiles of selected species concentrations at different times during the
785 simulation from Alt-Epping et al. (2006). The left and right panels are model scenarios without
786 and with ion exchange and biodegradation, respectively. The interface between borehole and
787 surrounding rock is marked by a vertical line. The profiles show that a greater complexity of
788 system processes entails a non-monotonous evolution of species concentration in the borehole.

789 Figure 3. Measurement of organic compounds as a function of time (TOC = total organic carbon,
790 DOC = dissolved organic carbon).

791 Figure 4. Measurements of methane concentrations as a function of time. a: bloom of
792 methanogenic activity. b: decrease in methanogenic activity.

793 Figure 5. Cl (open circles) and Br (closed circles) concentrations as a function of time.

794 Figure 6. $\frac{\{Na^+\}^z}{\{Me^{z+}\}}$ solute activity ratio as a function of time in the PC experiments (Me = K, Ca,

795 Mg and Sr).

796 Figure 7. Comparison between measurements (circles and red dashed line) and Br and HDO
797 modelled diffusion profiles. Plain and dashed curves are representative of calculations using
798 porosities of 75 or 100% of the measured total water content. Squares are representative of the
799 sample taken at day twelve while refilling the borehole. The pore diffusion coefficient (D_p)
800 remained unchanged at 0.9 and $2.4 \cdot 10^{-11} \text{ m}^2 \text{ s}^{-1}$ for anions and HDO respectively. Upper left
801 figure: Br concentration in the borehole as a function of time. Upper right figure: focus on the
802 initial stage of the experiment. Bottom left figure: HDO concentrations in the borehole as a
803 function of time. Bottom right figure: Br concentration ratio profile in the rock at the end of the
804 experiment. The distance is expressed in the bedding plane geometry (see Koroleva et al., this
805 volume).

806 Figure 8. Comparison of experimental results and model using glycerol as the organic carbon
807 source. Top left figure: organic matter. Plain line = acetate; dashed line = TOC (= acetate + solute
808 organic source). Top right figure: sulphate concentration. Bottom left figure: methane
809 concentration. Bottom right figure: evolution of kinetic rates as a function of time.

810 Figure 9. Saturation index of calcite as a function of time.

811 Figure 10. Left: total inorganic carbon (squares) and alkalinity (circles) as a function of time.
812 Right: pH (solid black line) as a function of time. Lines are indicative of modelled total inorganic
813 carbon and pH according to the following scenario (organic carbon release in solution / solid
814 source of carbon): 1- $\text{CH}_2\text{O}/\text{CH}_2\text{O}$; 2- Acetone / Acetone; 3- Glycerol / glycerol.

815 Figure 11. Left: total inorganic carbon (squares) and alkalinity (circles) as a function of time.
816 Right: pH (solid black line) as a function of time. Lines are indicative of modelled total inorganic
817 carbon and pH according to the following scenario (organic carbon release in solution / solid

818 source of carbon): 4- Glycerol / Glycerol without pH buffer of clay surfaces; 5- buffering
819 capacity $\times 3$; 6- porewater pH at 7.4 instead of 7.

820 Figure 12. Left: sulphide concentration as a function of time. Right: iron concentration as a
821 function of time (note that the concentration is in log scale). Lines are indicative of modelled
822 concentrations (Scenario 3 with glycerol).

823 Figure 13. Concentrations of major cations as a function of time. Circles: measurements. Lines:
824 model (Scenario 3 with glycerol).

825 Figure 14. Modelled pyrite (red) and amorphous sulphide (blue) solid concentration profile (in
826 mmol L^{-1} porewater) after 1846 days of perturbation (Glycerol simulation case).

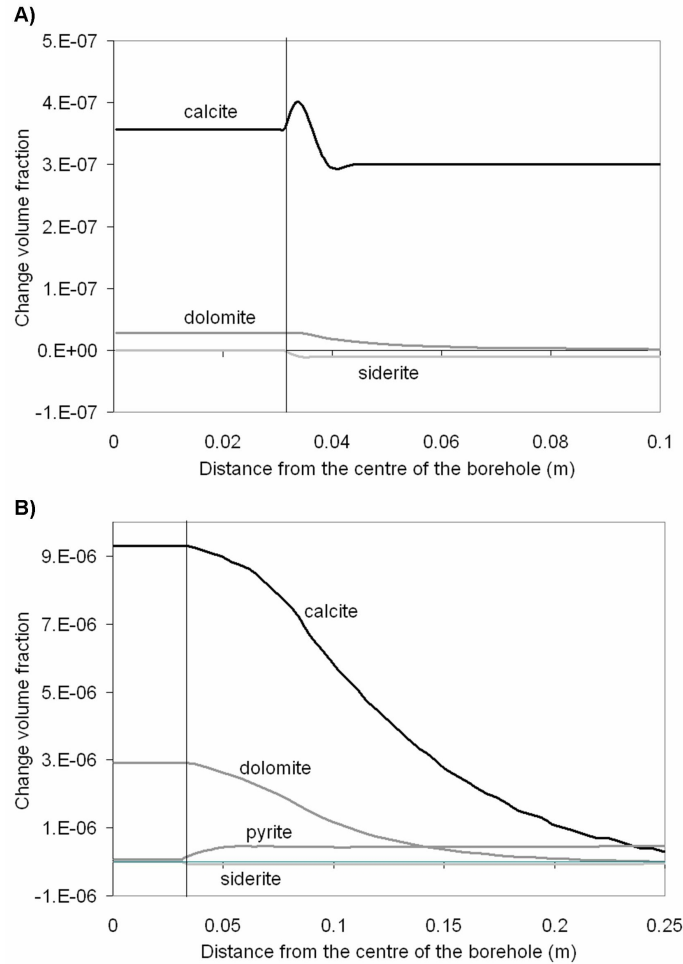
827 Figure 15. pH profile after 1846 days of perturbation (Glycerol simulation case).

828

829

830

831

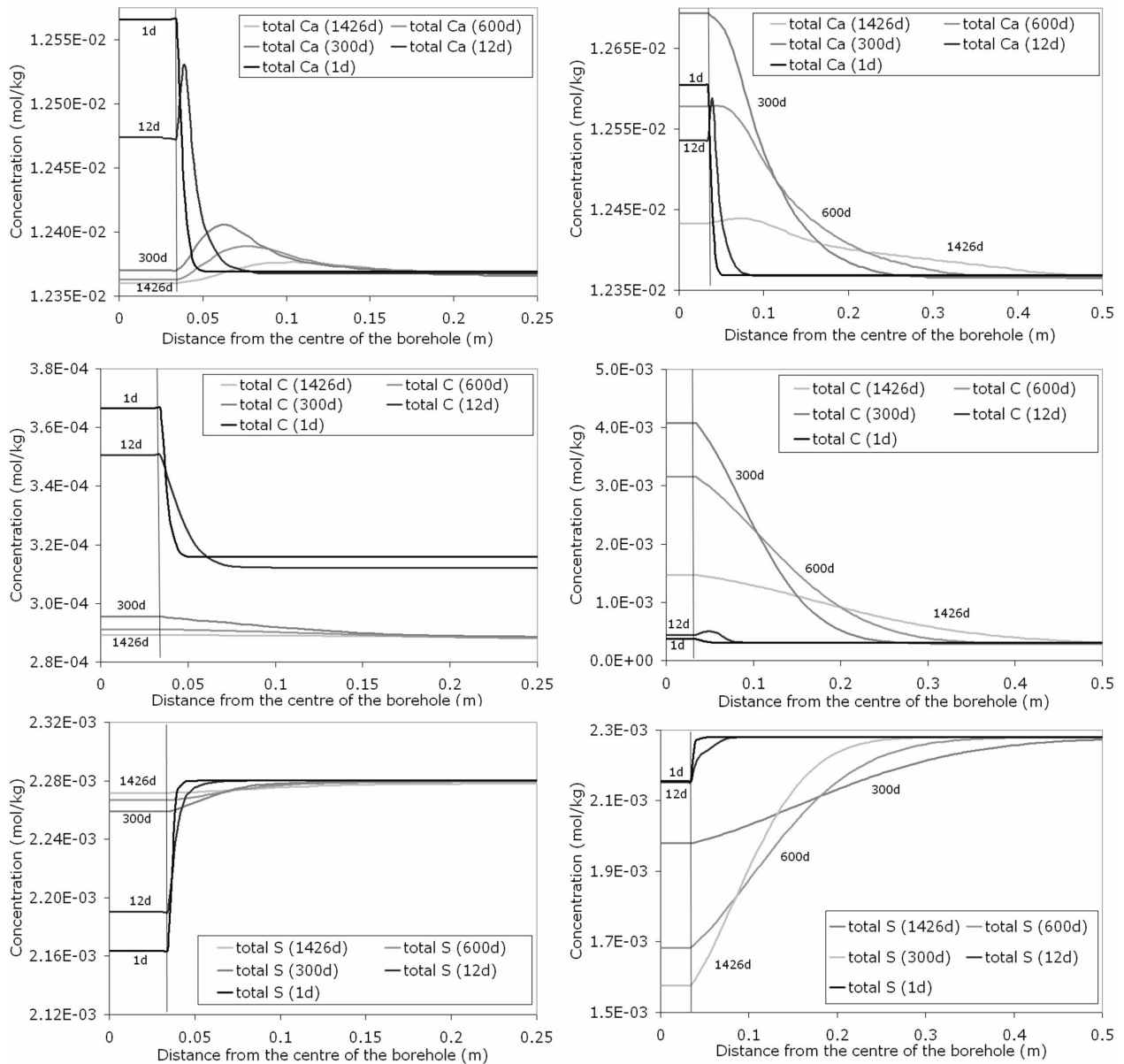


833

834 Figure 1. Profiles of mineral volume changes over a period of 1426 days, without (A) and with
 835 ion exchange and biodegradation (B) from Alt-Epping et al. (2006). The vertical line represents
 836 the borehole/rock interface. The precipitation of carbonate phases, calcite, dolomite and siderite
 837 along with ion exchange with clay surfaces act as buffer for the fluid composition. Increasing
 838 chemical complexity leads to a larger volume fraction of carbonate minerals. Sulphate reduction
 839 through biodegradation causes pyrite to precipitate.

840

841

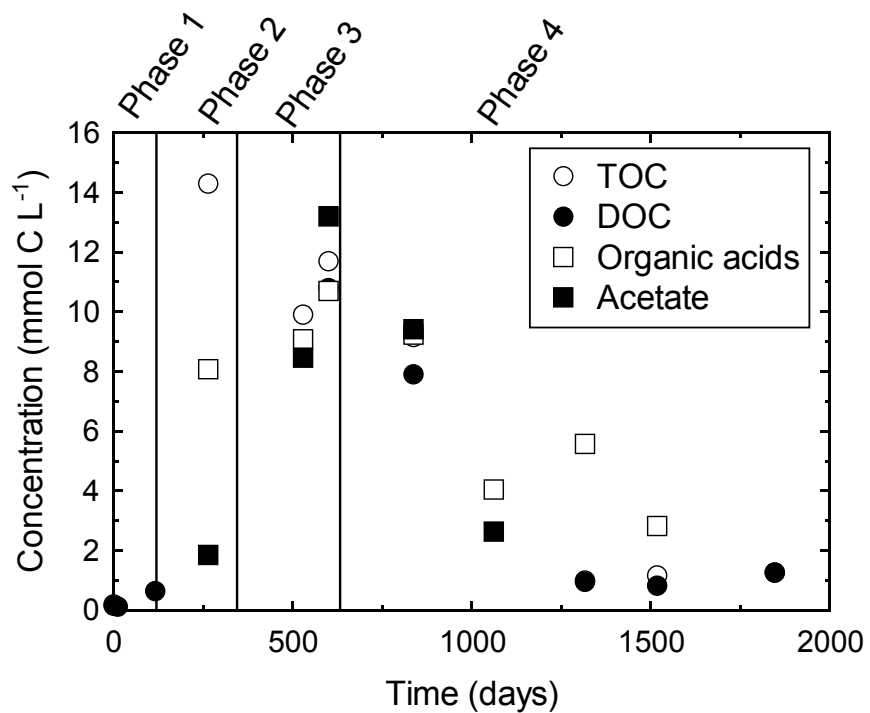


843

844 Figure 2. Spatial profiles of selected species concentrations at different times during the
 845 simulation from Alt-Epping et al. (2006). The left and right panels are model scenarios without
 846 and with ion exchange and biodegradation, respectively. The interface between borehole and
 847 surrounding rock is marked by a vertical line. The profiles show that a greater complexity of
 848 system processes entails a non-monotonous evolution of species concentration in the borehole.

849

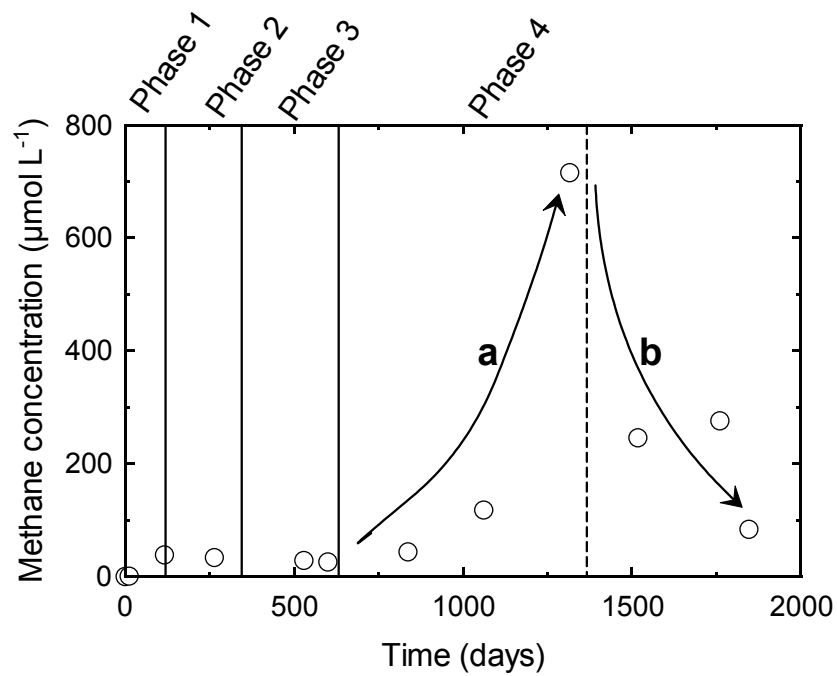
850



851

852 Figure 3. Measurement of organic compounds as a function of time in the borehole (TOC = total
853 organic carbon, DOC = dissolved organic carbon).

854



855

856 Figure 4. Measurements of methane concentrations as a function of time. a: bloom of
857 methanogenic activity. b: decrease in methanogenic activity.

858

859

860

861

862

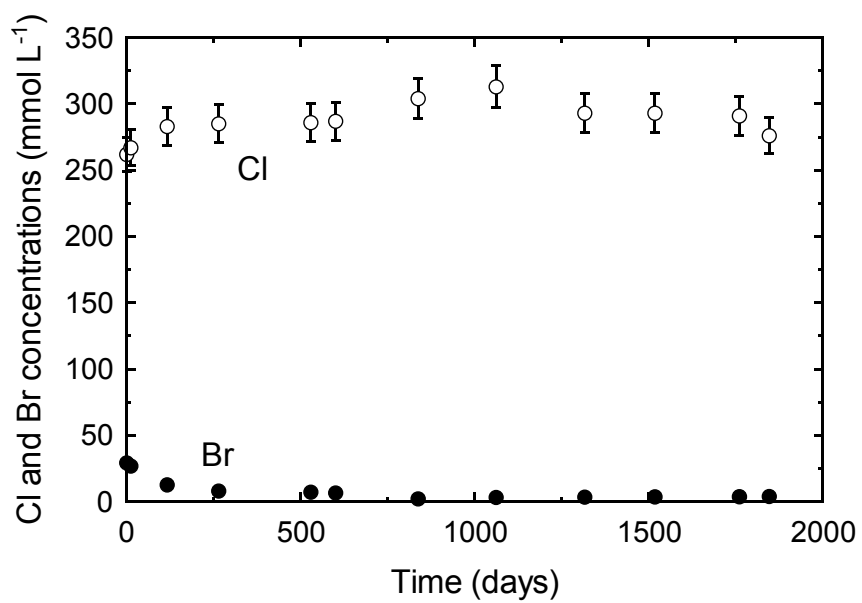


Figure 5. Cl (open circles) and Br (closed circles) concentrations as a function of time.

863

864

865

866

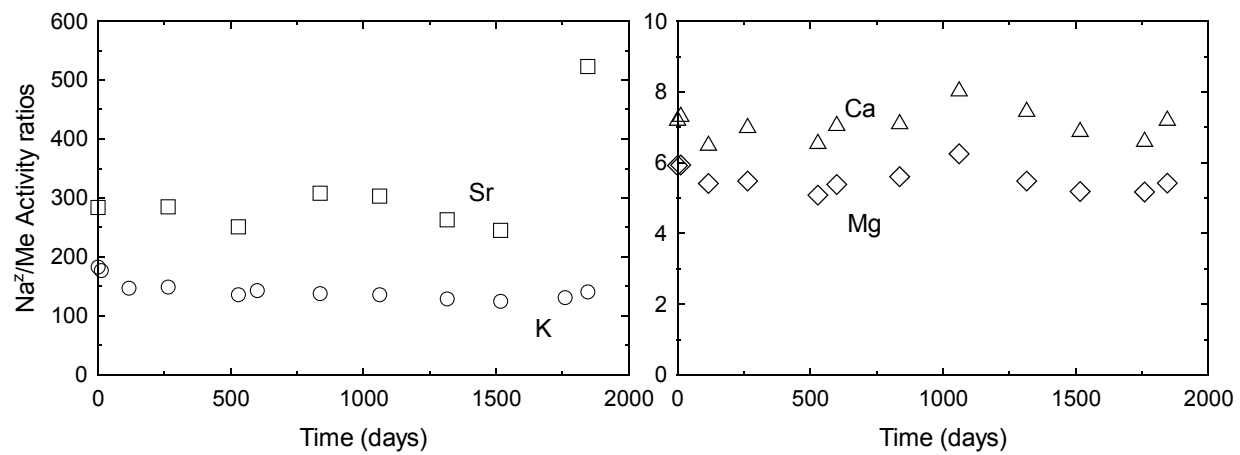
867

868

869

870

871



872

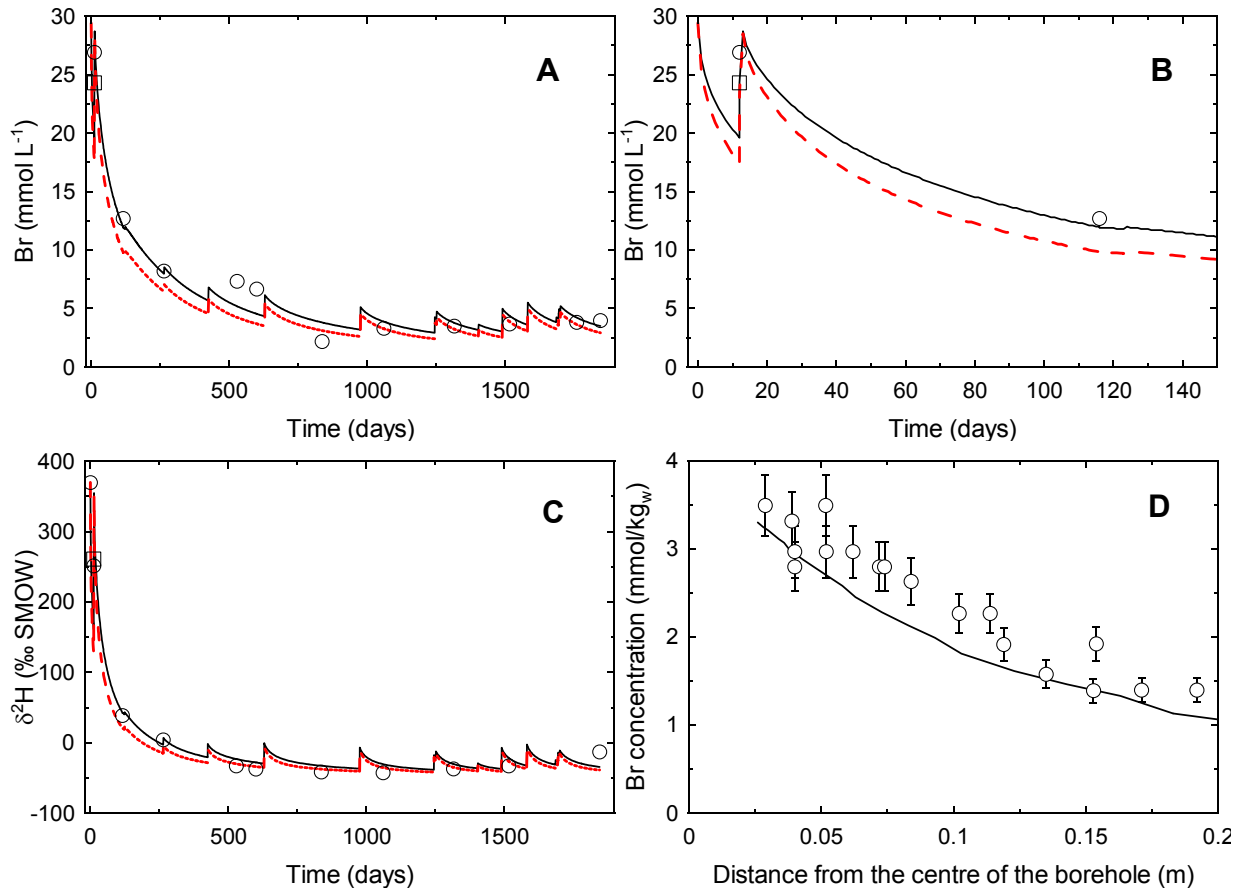
873 Figure 6. $\frac{\{Na^+\}^z}{\{Me^{z+}\}}$ solute activity ratio as a function of time in the PC experiments (Me = K, Ca,

874 Mg and Sr).

875

876

877



879

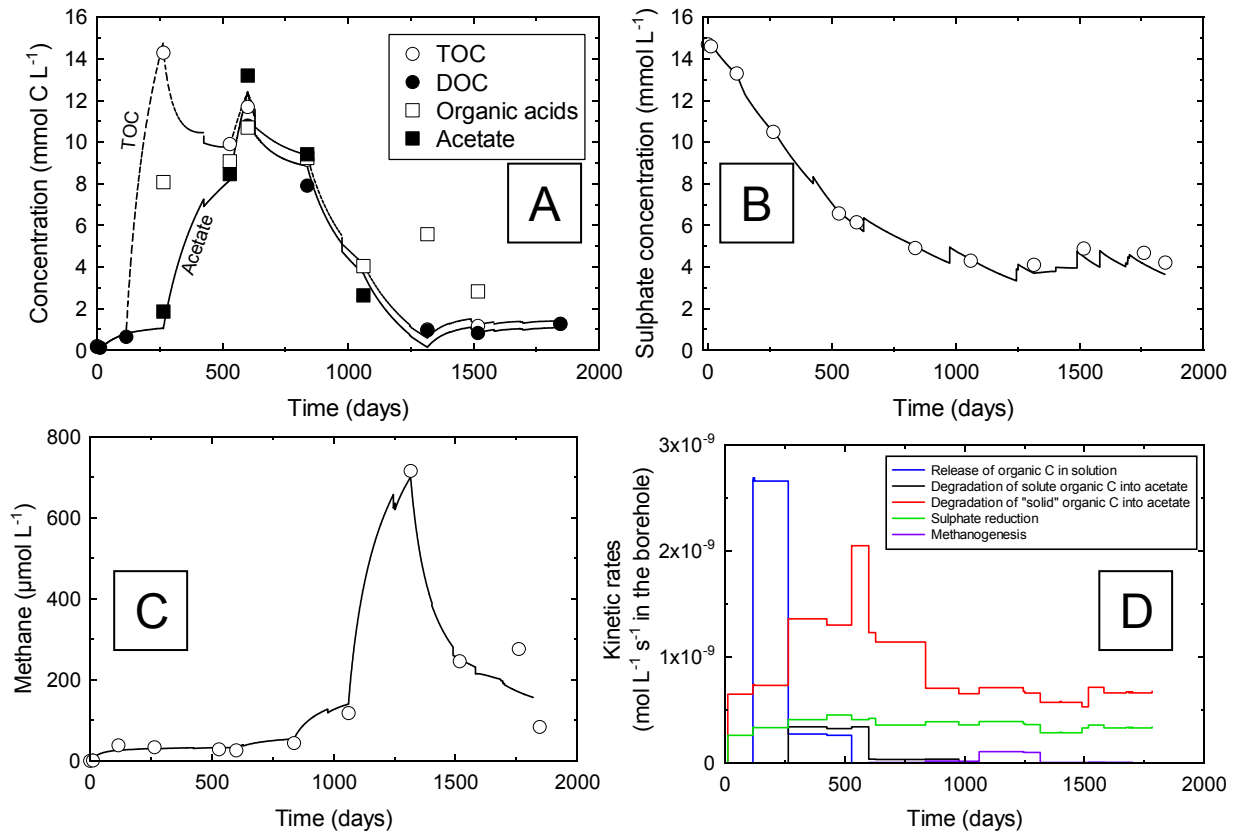
880

881

882 Figure 7. Comparison between measurements (circles) and Br and HDO modelled diffusion
 883 profiles (obtained from calibration). Black plain and red dashed curves are representative of
 884 calculations using porosities of 75 or 100% of the measured total water content. Squares are
 885 representative of the sample taken at day twelve while refilling the borehole. The pore diffusion
 886 coefficient (D_p) remained unchanged at 0.9 and $2.4 \cdot 10^{-10} \text{ m}^2 \text{ s}^{-1}$ for anions and HDO respectively.
 887 A: Br concentration in the borehole as a function of time. B: focus on the initial stage of the
 888 experiment. C: HDO concentrations in the borehole as a function of time. D: Br concentration
 889 ratio profile in the rock at the end of the experiment. The distance is expressed in the bedding
 890 plane geometry (Koroleva et al., This issue).

891

892



893

894 Figure 8. Comparison of experimental results and model using glycerol as the organic carbon

895 source. A: organic matter. Plain line = acetate; dashed line = TOC (= acetate + solute organic

896 source). B: sulphate concentration. C: methane concentration. D: evolution of kinetic rates as a

897 function of time.

898

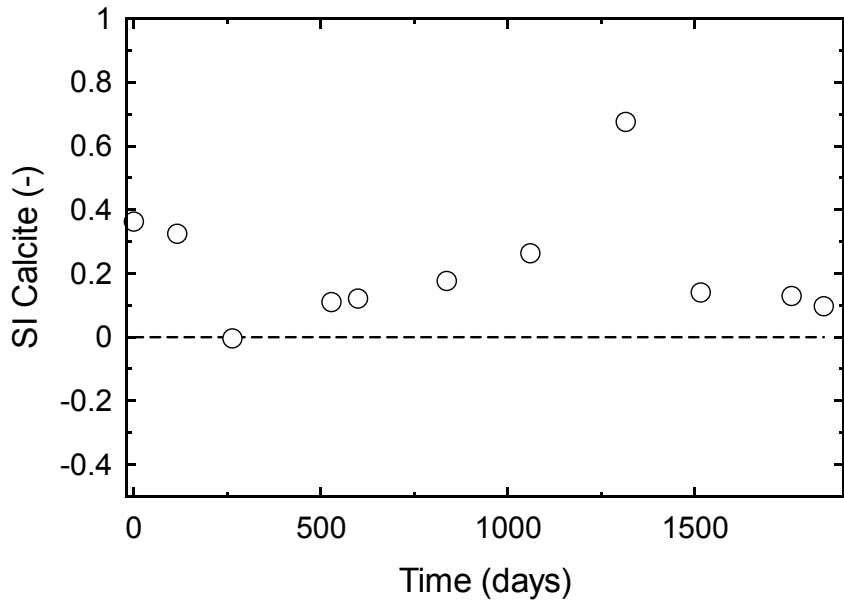
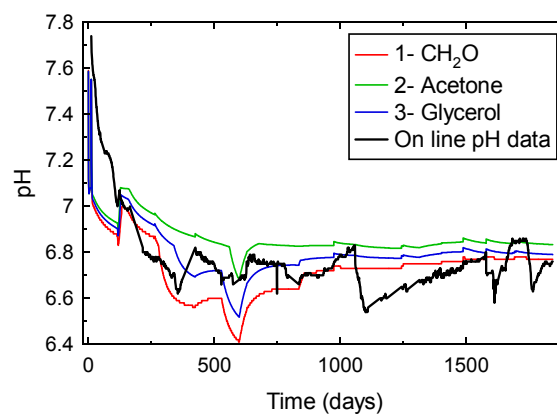
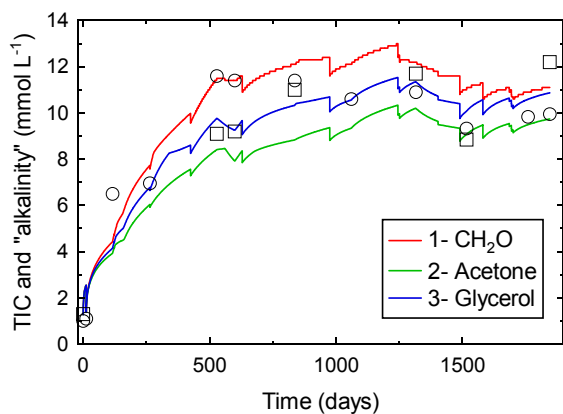


Figure 9. Saturation index of calcite as a function of time.

899
900
901
902
903
904
905
906
907
908



909

910

911 Figure 10. Left: total inorganic carbon (squares) and alkalinity (circles) as a function of time.

912 Right: pH (solid black line) as a function of time. Lines are indicative of modelled total inorganic

913 carbon and pH according to the following scenario (organic carbon release in solution / solid

914 source of carbon): 1- $\text{CH}_2\text{O}/\text{CH}_2\text{O}$; 2- Acetone / Acetone; 3- Glycerol / glycerol.

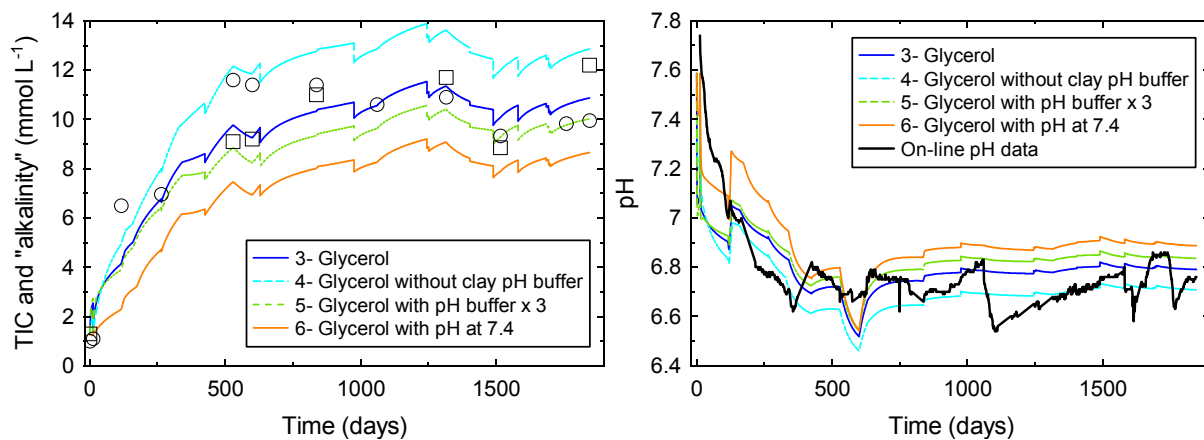
915

916

917

918

919



920

921

922 Figure 11. Left: total inorganic carbon (squares) and alkalinity (circles) as a function of time.

923 Right: pH (solid black line) as a function of time. Lines are indicative of modelled total inorganic

924 carbon and pH according to the following scenario (organic carbon release in solution / solid

925 source of carbon): 4- Glycerol / Glycerol without pH buffer of clay surfaces; 5- buffering

926 capacity $\times 3$; 6- porewater pH at 7.4 instead of 7.

927

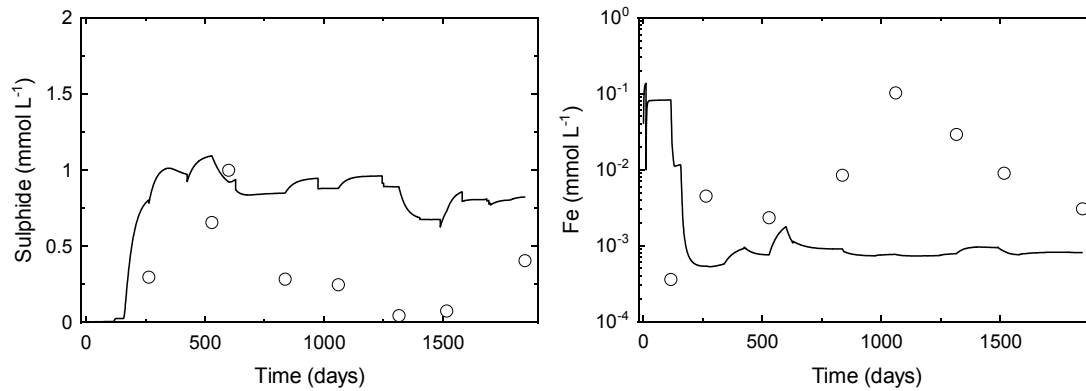
928

929

930

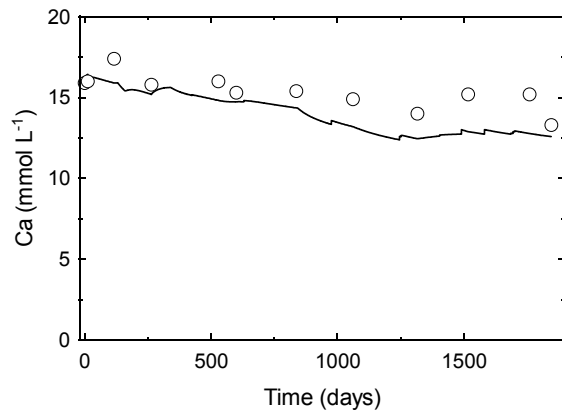
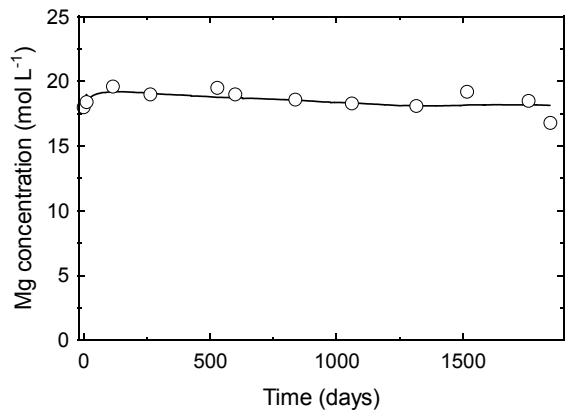
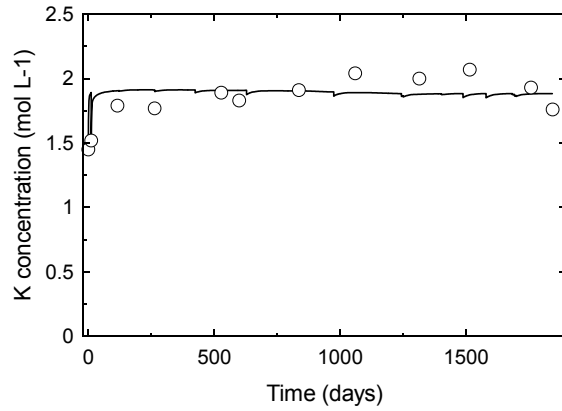
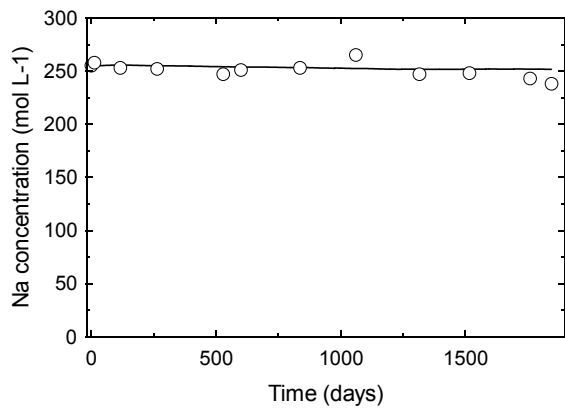
931

932



933
 934
 935 Figure 12. Left: sulphide concentration as a function of time. Right: iron concentration as a
 936 function of time (note that the concentration is in log scale). Lines are indicative of modelled
 937 concentrations (Scenario 3 with glycerol).

938
 939
 940
 941
 942
 943
 944
 945



946

947

948

949

950 Figure 13. Concentrations of major cations as a function of time. Circles: measurements. Lines:

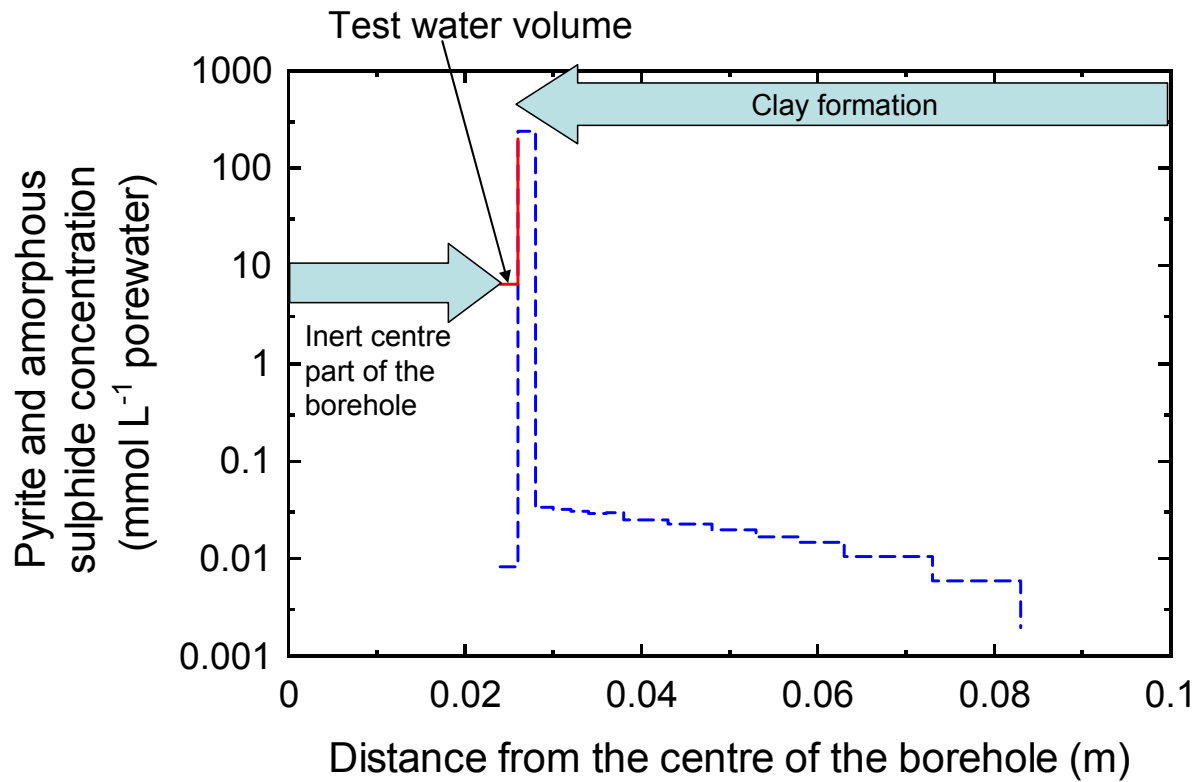
951 model (Scenario 3 with glycerol).

952

953

954

955



956

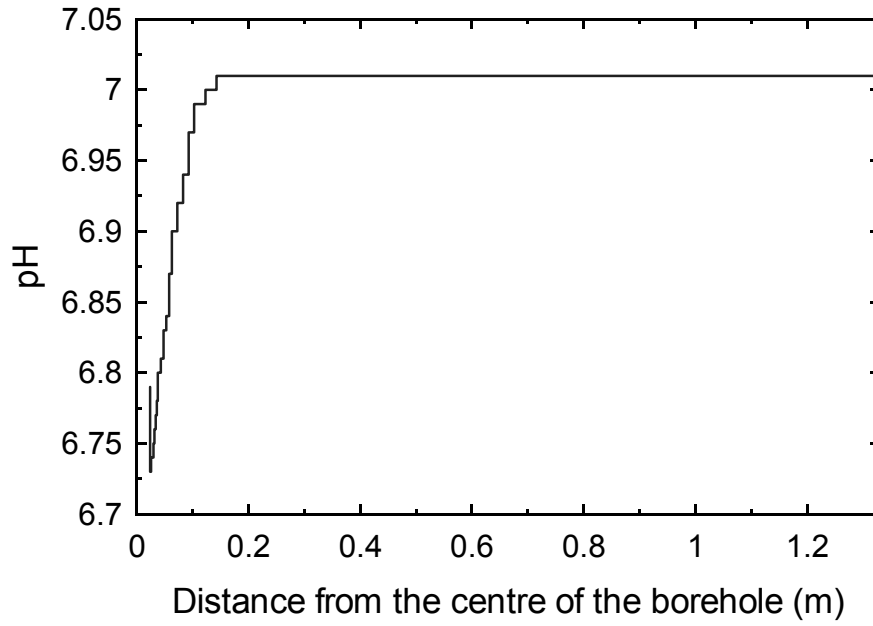
957 Figure 14. Modelled pyrite (red) and amorphous sulphide (blue) solid concentration profile (in
 958 mmol L^{-1} porewater) after 1846 days of perturbation (Glycerol simulation case).

959

960

961

962



963

964 Figure 15. pH profile after 1846 days of perturbation (Glycerol simulation case).

965

966